PALEONTOLOGY

Jurassic avialan reveals stepwise evolution of bony tail in birds

Min Wang[1]*†, Jianrong Tang[2]†, Ke Deng[2], Liping Dong[1], Liming Xu[2], Xing Xu[1], Min Lin[2], Honggang Du[2], Ganmin Lin[2], Runsheng Chen[2], Chi Zhang[1], Zhonghe Zhou[1]

The evolutionary assembly of the flight-adapted bird body plan encompasses some of the most profound morphological changes in terrestrial vertebrate history. Beyond feathered wings, the short pygostyle-bearing tail has been pivotal to the clade's ecological success. However, transition from the long bony tail to the short pygostyle-bearing tail remains a mystery, hindered by the scarcity of early branching avialans with transitional morphologies. Here, we report on a new avialan, *Zhengheornis buyu*, gen. et sp. nov., from the Upper Jurassic of southeastern China, suggesting that the vertebral reduction and shortening preceded pygostyle fusion in early avialan evolution, providing critical evidence for the stepwise evolution of the bird tail. *Z. buyu* is smaller than all known non-pygostylian paravians, expanding the species and body size diversity of stemward taxa.

INTRODUCTION

Distinguished from other reptiles including their dinosaurian ancestors, living birds have a short bony tail (*1*), which functions as a separate locomotor module with a high degree of evolutionary lability that contributes to their marked diversification (*1*–*3*). However, disentangling the transformation from the ancestral long bony tails of non-avialan dinosaurs and the earliest-diverging avialans to the short tails of pygostylian birds has been impeded by the exceeding rarity of early diverging avialans preserving intermediate morphologies (*4*–*6*). To further complicate matters, the fossil record shows near-simultaneous appearance of both long- and short-tailed avialans in equivalent spatiotemporal distribution in their earliest evolutionary stage (*5*, *7*). Developmental studies suggest that the fused pygostyle arose from pleiotropic effects of relatively a few mutations, arguing that the absence of stem avialans with intermediate tail morphologies may reflect a rapid evolutionary transition (*8*, *9*). Here, we address this issue by describing a previously unidentified avialan, *Zhengheornis buyu* gen. et sp. nov., from the Tithonian of China, which preserves an abbreviated tail comprising 15 short caudal vertebrae but no pygostyle. Our phylogenetic analyses resolve *Zhengheornis* as one of the earliest diverging avialans just crownward of *Archaeopteryx*. This specimen constitutes the fourth avialan discovered from the previously unrecognized Late Jurassic Zhenghe Fauna (*7*, *10*), and these taxa demonstrate varied morphologies and ecological adaptations. Together, these findings demonstrate that avialans were morphologically diverse by the end Jurassic (*11*–*13*).

RESULTS

Systematics

Theropoda Marsh, 1881. Maniraptora Gauthier, 1986. Avialae Gauthier, 1986. *Zhengheornis buyu* gen. et sp. nov. Etymology: "Zhenghe" (Mandarin), referring to Zhenghe Country, where the holotype specimen was found; "ornis," bird (Greek); "buyu," unexpected (Mandarin), from the ancient Chinese book *Guoyu*, referring to the unique tail and pelvic morphologies preserved in this species. Holotype: Institute of Vertebrate Paleontology and Paleoanthropology (IVPP) V34168, an articulated and partially complete skeleton (most limb bones are preserved as molds) with feathers preserved on a slab and counter slab (Fig. 1, figs. S1 and S2, and table S1). Locality and horizon: Near Yangyuan Village, Zhenghe Country, Nanping City, Fujian Province; Upper Jurassic, Nanyuan Formation [Tithonian stage; (*10*)]. Diagnosis: IVPP V34168 is distinguishable from all other paravians in the following combination of characters (*denotes probable autapomorphy): short tail comprising 15 vertebrae that is shorter than the hindlimb (combined length of femur, tibia, and metatarsal III)*; middle and posterior caudal vertebrae less elongate (opposite to the condition in other long tailed avialans); final two caudal vertebrae box-like*; manual phalanx III-1 shorter than III-2, opposite to the condition in *Archaeopteryx* and *Fujianvenator* [the three manual digits of maniraptorans are here identified as I, II, and III, as in (*14*)]; manual phalanx III-3 50% longer than III-2 (the length ratio greater than 2 in *Anchiornis* and *Archaeopteryx*); slender ischium that has a knob-like, distally located obturator process and lacks the posterior process*; short fibula that terminates far proximal to the ankle; metatarsal I that articulates at the distal third of metatarsal II; metatarsal II that ends far proximal to metatarsal III trochlea; short hallux with an ungual that is smaller than that of other pedal digits; and robust digit II that has the longest non-ungual (II-2) and ungual pedal phalanges.

Description

The holotype of *Zhengheornis* is a small avialan. We interpreted IVPP V34168 to be subadult or adult on the basis of fused synsacrum and tibiotarsus, considering that fusion of these elements occurred in late developmental stage in early avialans (*15*, *16*). IVPP V34168 is estimated to have a body mass of ~74 to 163 g using empirical equations on basis of femoral midshaft circumference (Materials and Methods) (*17*, *18*). Complete measurements of IVPP V34168 are provided in table S1.

The trunk posterior to the shoulder is complete and articulated (Fig. 1 and fig. S1). The middle and posterior dorsal vertebrae have basally constricted neural spines that are dorsoventrally higher than the centrum height, but the opposite is true in other Jurassic paravians such as *Fujianvenator* (*10*), *Archaeopteryx* (*19*), and *Caihong* (*20*). The ventral margin of the dorsal centrum is concave in lateral

[1]Institute of Vertebrate Paleontology and Paleoanthropology, Chinese Academy of Sciences, Beijing 100044, China. [2]Fujian Province Geological Science Research Institute, Fuzhou 350013, China.
*Corresponding author. Email: wangmin@ivpp.ac.cn
†These authors contributed equally to this work.

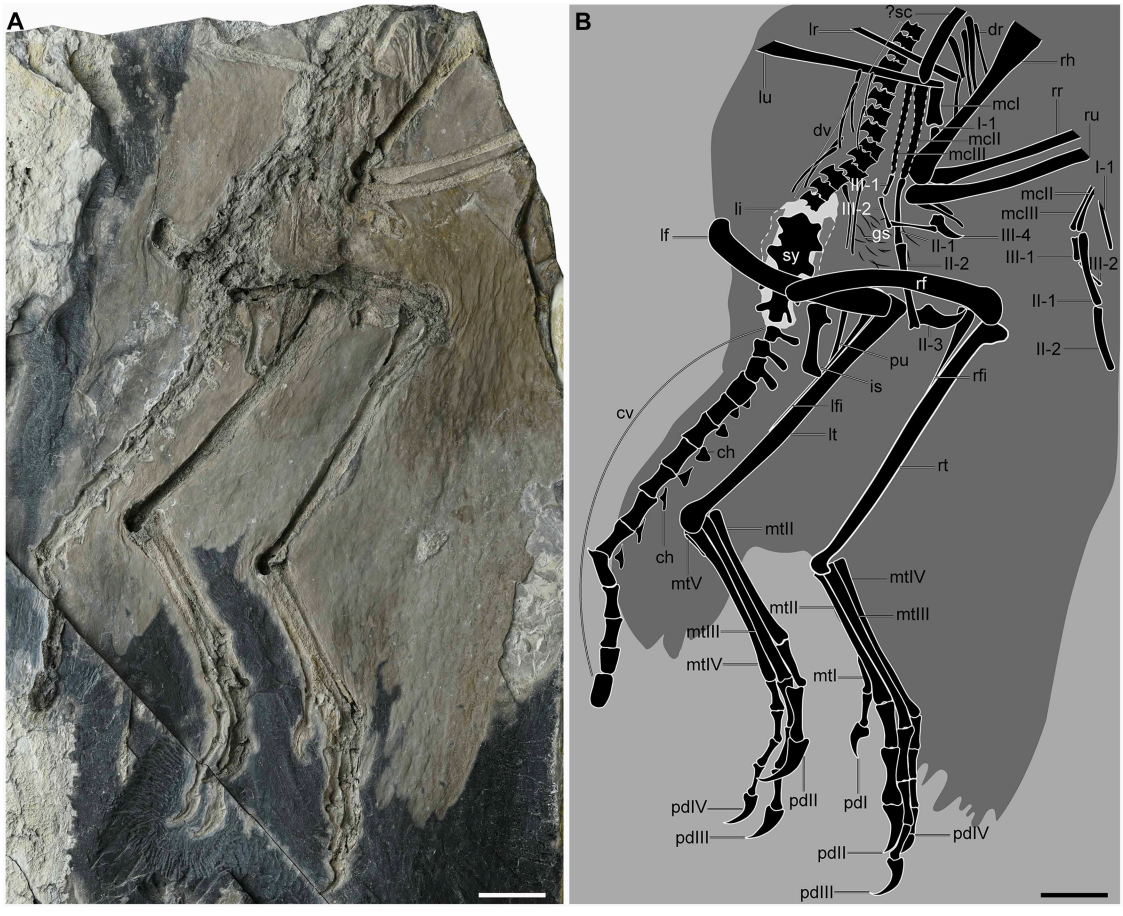

Fig. 1. Holotype of *Zhengheornis buyu*, IVPP V34168. (**A** and **B**) Photograph (A) and line drawing (B) of the holotype of *Z. buyu* (IVPP V34168). ch, chevron; cv, caudal vertebra; dr, dorsal rib; dv, dorsal vertebra; gs, gastralia; is, ischium; lf, left femur; lfi, left fibula; li, left ilium; lr, left radius; lt, left tibia; lu, left ulna; mcI to mcIII, metacarpal I to III; mtI to mtV, metatarsal I to V; pdI to pdIV, pedal digit I to IV; pu, pubis; rh, right humerus; rf, right femur; rfi, right fibula; rr, right radius; rt., right tibia; ru, right ulna; ?sc, possible scapula; sy, synsacrum; I-1, manual phalanx I-1; II-1 to II-3, manual phalanx II-1 to II-3; III-1 to III-4, manual phalanx III-1 to III-4. Scale bars, 10 mm [(A) and (B)].

view. The synsacrum probably consists of five sacrals, comparable to that of other early paravians (*20*–*23*), but fewer than in crownward avialans (*24*). The last sacral has a pair of elongate posterolaterally directed transverse processes. The complete tail consists of 15 vertebrae (Fig. 2, A and B). Considering the proximity of the synsacrum and the caudal vertebrae, and the articulated vertebral column, one or two additional anterior-most caudal vertebrae might have been present. Nevertheless, the tail is notably shorter than in other long-tailed paravians in terms of both vertebral count and relative length. Specifically, there are 23 to 24 caudals in *Archaeopteryx* (*25*, *26*), 22 to 27 in *Jeholornis* (*24*), and >30 in other early paravians such as anchiornithines and *Jianianhualong* (fig. S3 and table S2) (*20*, *22*, *23*, *27*, *28*). The tail measures only two-thirds of the length of the hindlimb (combined length of femur, tibia, and metatarsal III), contrasting with the fact that the tail is longer than the hindlimb in most other long-tailed paravians (tables S3 and S4) (*4*, *19*, *22*, *24*, *29*). As in stem paravians (*22*, *30*, *31*), the anterior caudal vertebrae are much shorter than the posterior dorsal vertebrae. Transverse processes are only developed on the anterior five caudal vertebrae, indicating that the transition point occurs around the sixth caudal vertebra as in *Archaeopteryx* and *Anchiornis* (*22*, *24*), whereas in deinonychosaurs, it is located posteriorly to the 9th to 10th vertebrae (fig. S4) (*4*, *32*, *33*). Some oviraptorosaurians and scansoriopterygids such as *Ambopteryx*, although having a short tail with most caudal vertebrae bearing transverse processes, lack a clearly defined transition point (*4*, *34*). As in *Anchiornis* and troodontids (*32*, *35*), the transverse processes are slender, contrasting with the distally flared condition seen in *Archaeopteryx* and dromaeosaurids (fig. S4, A to E) (*21*, *33*). The vertebrae posterior to the transition point are less elongate than in other early paravians such as *Fujianvenator* and *Archaeopteryx*, in which the centra are more than four times as long as they are wide (fig. S4) (*4*, *10*, *19*, *22*). The two terminal vertebrae differ greatly from preceding ones in being box-like and having bluntly convex caudal ends. All these features compare favorably with *Caudipteryx* (figs. S5, A and B, and S6) (*4*). The 14th and 15th caudals are proportionally shorter than proximal ones (the length/depth ratio is 1.4, compared with greater than 2 in 10th to 13th caudals; table S1). By contrast, in other long-tailed paravians and scansoriopterygids, the vertebrae in equivalent positions are splint-like, with a length/depth ratio greater than 3 (figs. S4 and S5, C and D) (*23*, *24*, *27*, *36*, *37*). Although the caudalmost two caudals are not well preserved, the overall preservation of IVPP V34168 (most bones remain articulated, and no other vertebra-like elements are found on both slabs) suggest that additional vertebrae posterior to the 15th caudal are unlikely to be present. Moreover,

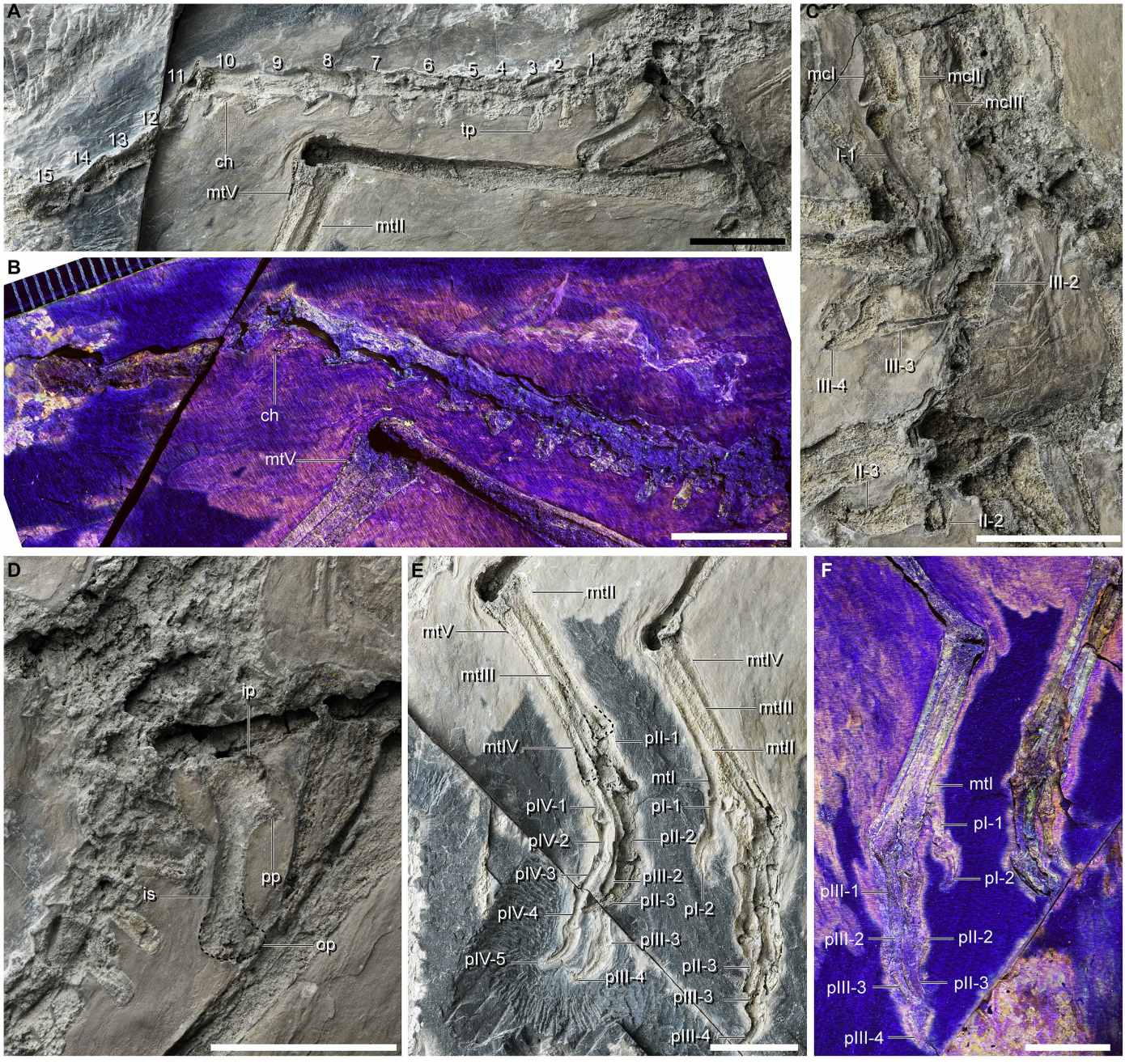

Fig. 2. Anatomy of *Z. buyu*, IVPP V34168. (**A** and **B**) Caudal vertebrae under normal (A) and laser light (B). The numbers 1 to 15 denote the free caudal vertebrae. (**C**) Left manus. (**D**) Pelvic girdle. (**E** and **F**) Feet under normal (E) and laser light (F). ch, chevron; is, ischium; ip, iliac peduncle of ischium; mcI to mcIII, metacarpal I to III; mtI to mtV, metatarsal I to V; op, obturator process; pI-1 to pI-2, pedal phalanx I-1 and I-2; pII-1 to II-3, pedal phalanx II-1 to II-3; pIII-1 to III-4, pedal phalanx III-1 to III-4; pIV-1 to IV-5, pedal phalanx IV-1to IV-5; pp, pubic peduncle of ischium; tp, transverse process; I-1, manual phalanx I-1; II-2 to II-3, manual phalanx II-2 and II-3; III-2 to III-4, manual phalanx III-2 to III-4. Scale bars, 10 mm [(A) to (F)].

there are no avialan or non-avialan theropods that show similar caudal morphology (suddenly changing from splint-like to box-like form) in the middle or posterior region of the tail (fig. S4). In contrast, such box-like and bluntly ended caudals are seen in the end of the tail in *Caudipteryx*. Therefore, we posit that the 14th and 15th caudals are genuinely the caudalmost caudals. The terminal caudals are unfused with one another. Given the relatively skeletal maturity of IVPP V34168, the unfused condition cannot be ascribed to ontogeny. As in *Archaeopteryx* and *Anchiornis* (*22*, *36*), the anterior chevrons are dorsoventrally deep and rectangular, rather than being rod-like as in many deinonychosaurians and oviraptorosaurs (Fig. 2A and fig. S4) (*22*). The middle and posterior chevrons are elongate anteroposteriorly, but to a lesser extent than in other paravians in which the hyperelongated chevrons contact with each other such as in *Anchiornis*,

Jeholornis, and deinonychosaurians (fig. S4) (*19*, *22*, *24*, *32*, *33*, *38*). Specifically, the chevron located posterior to the 10th caudal is relatively shorter than in *Archaeopteryx* [the depth/length ratio is 0.47, compared with 0.27 in the latter taxon; (*19*)]. No uncinate processes are preserved, as in other stem avialans. The slender gastralia are nearly straight and taper at both ends.

The humerus is weakly expanded dorsoventrally at its distal end. As in *Archaeopteryx* (*36*), but not in *Anchiornis* or *Fujianvenator* (*10*, *22*), the ulna is bowed dorsally (Fig. 1). Quill knobs for the attachment of the remiges are absent, a plesiomorphic condition for avialans (*31*, *36*, *39*, *40*). The straight radius measures 85% of the width of the ulna. The manus retains the ancestral theropod condition in having a phalangeal formula of 2-3-4 (Fig. 2C and fig. S7A) (*12*, *39*). As in other early paravians (*7*, *10*, *22*, *41*), metacarpal I lacks an extensor process and ends in a ginglymoid articulation. The unguals are strongly curved and have prominent flexor processes. Phalanx II-2 is longer than II-1, a primitive condition of avialans (*19*, *39*). As in *Anchiornis* and *Caihong* (*20*, *22*), phalanx III-1 is slightly shorter than III-2, but the opposite is true in other stem avialans, including *Fujianvenator*, *Archaeopteryx*, and *Baminornis* (fig. S7 and table S3) (*7*, *10*, *19*). Phalanx III-3 is 1.5 times as long as III-2, comparable to that of *Baminornis* (*7*)—proportionately shorter than in other Jurassic avialans (table S3) (*10*, *19*, *27*).

The strap-like ischium is slender and lacks the prominently expanded distal end that is present in other non-avialan theropods and Jurassic avialans (Fig. 2D and fig. S5, E, F, and H) (*10*, *28*, *30*, *35*, *42*). As in *Fujianvenator*, *Anchiornis*, and *Archaeopteryx* (*10*, *31*), the obturator process is distally located, but lacks the constriction at its base that is characteristically present in the former three taxa (fig. S5, H to K). By contrast, the obturator process is more proximally located in many dromaeosaurids and troodontids (*32*, *33*). The small obturator process is knob-like, which contrasts with both the rectangular form, seen in *Anchiornis* and *Archaeopteryx* (*21*, *31*), and the triangular form, seen in *Fujianvenator* and non-avialan coelurosaurians (*10*, *30*, *42*). The obturator process is independently lost in scansoriopterygids and later avialans (*30*, *37*). As in *Anchiornis* and *Baminornis* (*7*, *31*), the ischium lacks the posterior process that is widely distributed among early paravians, with two in *Archaeopteryx* and deinonychosaurians (*31*–*33*), and one in *Fujianvenator* and many Cretaceous avialans (fig. S5) (*10*, *43*, *44*). As in some deinonychosaurs (*28*, *31*, *42*), the ischium ends bluntly posteriorly, rather than tapering into a pointed posterior end as in *Fujianvenator*, *Anchiornis*, and *Archaeopteryx* (fig. S5, E to K) (*10*, *25*, *31*). The pubis is rod-like.

The robust femur measures 70% of the length of the tibia, comparable to that of *Archaeopteryx* and *Anchiornis* (*19*, *22*), but proportionately longer than in *Fujianvenator* (table S3) (*10*). The tibia is straight laterally. Both tibiae are preserved in articulation with the proximal tarsals with little displacement, suggesting that these elements are partially or fully fused into a tibiotarsus (Figs. 1 and 2, E and F). Unlike other Jurassic paravians and most non-paravian theropods (*10*, *19*, *45*), the fibula ends far proximal to the ankle (Fig. 1 and fig. S1), a derived feature previously known in avialans from the Cretaceous onward (*45*). A short fibula is convergently developed in some Late Cretaceous alvarezsaurids and oviraptorosaurs (*46*). As in early avialans (*10*, *47*), the metatarsus is gracile (Fig. 2, E and F), contrasting with the stout form that is seen in many non-paravian theropods and Cretaceous avialans such as *Jeholornis* and confuciusornithids (*39*, *43*, *47*). Metatarsals II to IV are unfused with one another or with the distal tarsals, a plesiomorphic condition of avialans (*39*, *48*). Metatarsal I articulates with the posteromedial side of metatarsal II at its distal third-length (Fig. 2E and fig. S2), whereas it is more distally located in other early paravians except *Fujianvenator* (*10*, *47*–*49*). Metatarsal III is the longest, followed by metatarsal IV, and metatarsal II terminates far proximal to the proximal margins of the trochleae of metatarsals III and IV (Fig. 2F). This configuration is unique among early paravians. For instance, metatarsal II is either slightly shorter than or as along as metatarsal IV in *Archaeopteryx*, *Fujianvenator*, *Anchiornis*, and some dromaeosaurids (*10*, *21*, *22*, *30*, *47*), whereas in troodontids metatarsal IV is characteristically longer than other metatarsals (*32*, *50*). As in *Fujianvenator* and *Anchiornis* (*10*, *22*)—but unlike *Archaeopteryx* and many non-avialan theropods (*21*, *30*)—metatarsal III is not pinched proximally. Like many enantiornithines (*44*), metatarsal III is the most robust metatarsal, and metatarsal IV is narrower than metatarsal II. By contrast, metatarsal II is stouter than other metatarsals in other Jurassic avialans and some dromaeosaurids (*10*, *19*, *33*), but in troodontids, metatarsal IV is the most robust metatarsal (*32*). The reduced metatarsal V measures one-sixth of the length of metatarsal III (Fig. 2E), proportionately shorter than in *Archaeopteryx* and *Anchiornis* (*19*, *22*).

The hallux is notably short (Fig. 2, E and F). Phalanx I-1 is less than two-thirds of the length of II-1. The hallucal ungual is smaller than that of other digits, as in *Xiaotingia* and *Anchiornis* (*31*, *35*). A short phalanx I-1 is the ancestral condition of maniraptorans (*22*), which is relatively long in *Archaeopteryx* and is longer than II-1 in more crownward taxa such as *Jeholornis* and jinguofortisids (*19*, *24*, *41*). In *Archaeopteryx* and many crownward taxa, the hallucal ungual is no smaller than that of digit IV (*19*, *40*, *41*). In contrast to what is observed in other Jurassic avialans (*19*, *22*), digit II is more robust than digit III, as in some enantiornithines (*40*). The longest non-ungual phalanx is II-2, rather than being III-1 as in other Jurassic avialans (e.g., *Archaeopteryx*, anchiornithines) (*19*, *22*, *23*), whereas in most deinonychosaurs, phalanx II-2 is shorter than II-1 (*32*, *33*). Phalanx II-2 readily differs from that of *Archaeopteryx*, anchiornithines, and deinonychosaurs in lacking the features associated with hyperextension, including the proximoventral heel and the distal articulation that expands dorsally and bears dorsally located lateral ligament fossa (Fig. 2F) (*31*–*33*). As in *Archaeopteryx* and *Anchiornis* (*19*, *22*), the phalangeal lengths of digit III decrease distally.

The entire skeleton is surrounded by a halo of feather traces (Fig. 1 and fig. S1), which also extend down the proximal part of the metatarsus, as in other early avialans (*35*). The remiges terminate with pointed ends and appear to be asymmetrical. Features of the rectrices are hardly recognizable.

Morphometric analyses

To explore the ecological adaptation of *Zhengheornis*, phylogenetically corrected morphometric analyses were conducted to compare hindlimb proportions among Mesozoic theropods (Supplementary Materials). The results of phylogenetic principal components analysis (pPCA) using measurements of femur, tibia, and metatarsal III show that *Zhengheornis* is placed in an intermediate position between non-avialan and avialan theropods along principal component (PC) 1 (Fig. 3, A to C and fig. S8A). PC 1 correlates negatively with all variables with approximately equal eigenvector coefficients, indicating that it captures elongation of the hindlimb and thus correlates with body size (table S5). PCs 2 and 3 describe the elongation of the femur and metatarsal III relative to other elements, respectively. Non-avialan and avialan theropods overlap substantially along these axes

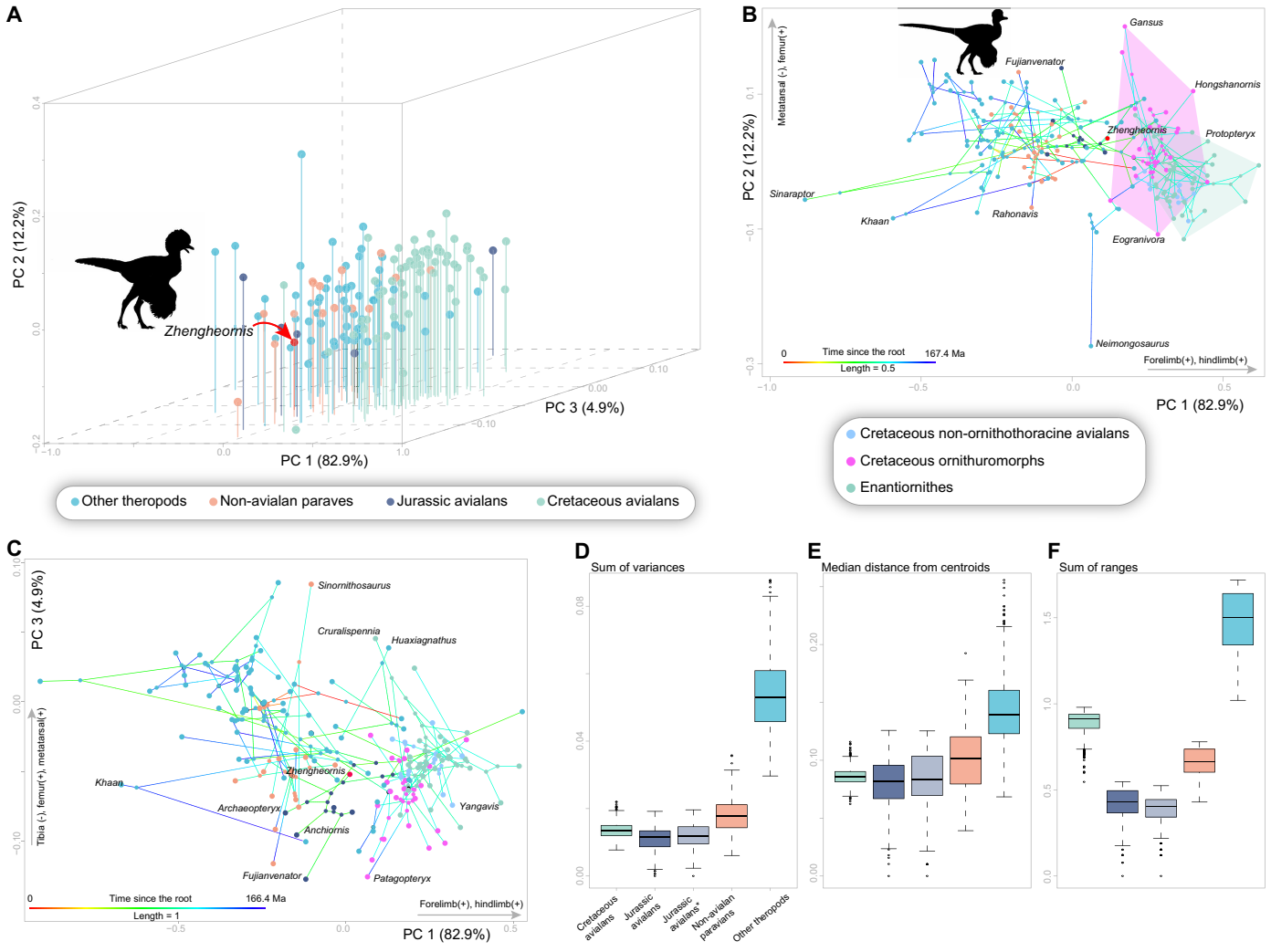

Fig. 3. Morphospace and hindlimb disparity of Mesozoic theropods. (**A** to **C**) Phylogenetic morphospace based on the first three PCs (A) and two PCs [(B) and (C)] derived from pPCA. See fig. S8 for additional results. The phylogenetic tree is superimposed onto the morphospace by uniting taxa based on their evolutionary relationships. (**D** to **F**) Comparison of hindlimb disparity of subgroups of Mesozoic theropods (*denotes results without *Zhengheornis*). The boxes indicate the median and the first and third quartiles of morphological disparity (n = 138 independent taxa).

(Fig. 3, B and C, and fig. S8A). Enantiornithines and ornithuromorphs are separated from each other along PCs 2 and 3, reflecting their contrasting ecological preferences—arboreal and terrestrial (*51*). *Zhengheornis* falls in the intermediate position between enantiornithines and ornithuromorphs, and it is located far away from *Archaeopteryx*, *Anchiornis*, and *Fujianvenator*, which plot near the morphospace of ornithuromorphs (Fig. 3, B and C, and fig. S8A). Similar results are recovered with conventional PCA, and pPCA focusing on Mesozoic avialans (figs. S7 and S8 and tables S6 and S7). The discovery of *Zhengheornis* brings nuanced impacts on the hindlimb disparity of Jurassic avialans. Quantitative metrics that describe the average dissimilarity among species (sum of variance and the median distance from centroids) change little with and without *Zhengheornis* (*52*), whereas *Zhengheornis* increases the disparity of Jurassic avialans in terms of sum of ranges, which reflects the overall distribution of hindlimb proportion (Fig. 3D) (*53*). Rarefaction analyses showed that these results are not strongly affected by sampling bias (fig. S10). The morphometric analyses and the lack of clear morphological features for terrestrial or arboreal adaptations (e.g., short and proximally located hallux, less elongate tibia, weakly curved unguals) suggest that *Zhengheornis* was not well adapted to neither habitats, a niche preference different from other Jurassic avialans, particularly the co-occurring long-legged *Fujianvenator* (*10*, *13*).

DISCUSSION

Our phylogenetic analyses consistently recovered *Zhengheornis* as one of the earliest diverging avialans that is just crownward of the anchiornithines and *Archaeopteryx*, a result that is corroborated by maximum parsimony and Bayesian tip-dating analyses (Fig. 4A and figs. S11 and S12). Referral of *Zhengheornis* to the Avialae is supported by two synapomorphies, and one of them can be accessed in IVPP V34168: transition point located proximal to the seventh caudal vertebra (character state 114.2). The more crownward position of *Zhengheornis* relative to *Archaeopteryx* is supported by three synapomorphies, and two of them can be scored: metatarsal II ending

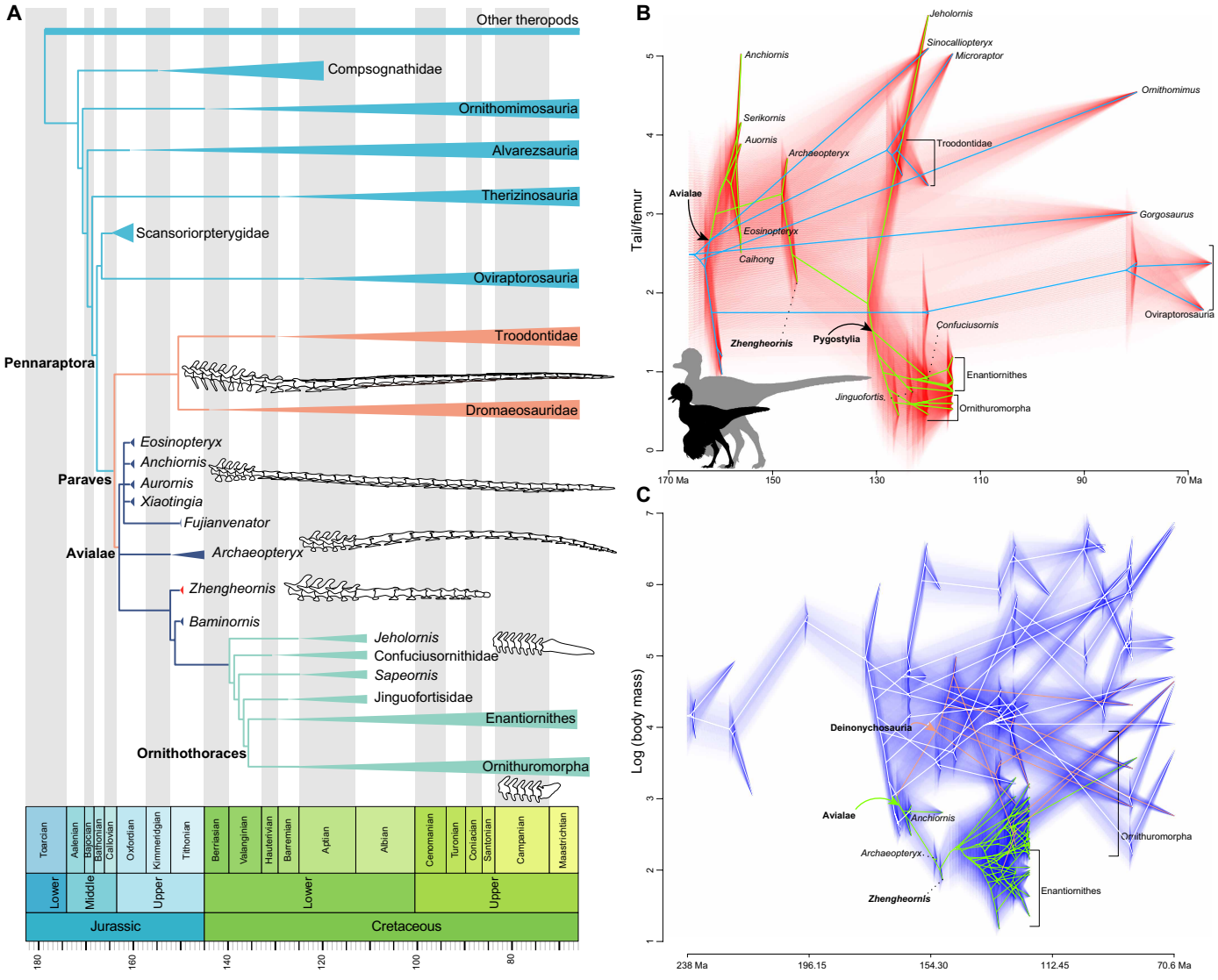

Fig. 4. Phylogeny, tail length, and body mass evolution of Mesozoic theropods. (**A**) Time-scaled phylogeny showing the position of *Z. buyu*. See figs. S11 and S12 for complete results of phylogenetic analyses. (**B** and **C**) Traitgrams projecting the Mesozoic theropod phylogeny into a space derived from the relative tail length (B) and body mass variations (C) through evolutionary time. The vertical position of nodes shows reconstructed ancestral state for the length ratio of tail/femur (B) and body mass (C), and the horizontal position denotes time from the root. Uncertainty is depicted via increasing transparency of orange (B) and blue (C) lines along branches and at notes, which indicate 95% confidence interval of point estimates. Silhouettes of *Zhengheornis* (in dark) and *Fujianvenator* (in gray) are superimposed to highlight the short tail and small size of *Zhengheornis*. See figs. S13 and S14 for complete results with species name.

distally only as far as the base of metatarsal IV trochlea (character state 433.2) and distal end of humerus less than twice the width of its shaft (character state 796.1). Considering the exceedingly rare fossil record of the earliest diverging avialans, *Zhengheornis* not only increases the known diversity of Jurassic avialans, but, more importantly, also fills a morphological gap between the ancestral long bony-tailed avialans and the derived short-tailed pygostylians. For instance, the ischium, although bearing an obturator process, is much slender than in most other Jurassic avialans (fig. S5, H to K), and the fibula terminates far proximal to the distal end of the tibia (Fig. 1), a derived feature previously known in pygostylians (*45*).

Acquisition of the characteristic bird body plan involves numerous changes in musculoskeletal and epidermal structures, some of which stand as unrivaled morphological innovations in terrestrial vertebrate evolution (*12*, *51*, *54*). Among these, a short pygostyle-bearing tail is functionally and ecologically vital to living birds, which enables tail fanning and conveys aerodynamic advantages (*2*, *54*–*56*). The continuing discoveries of stemward avialans and their kin have demonstrated the short-lived coexistence of long- and short-tailed avialans in equivalent spatiotemporal distribution (*4*–*6*), exemplified by the recent discoveries of *Fujianvenator* and *Baminornis* from the Late Jurassic Zhenghe Fauna (*7*), wherein the long-tailed Early Cretaceous *Jeholornis* has more caudal vertebrae than *Archaeopteryx*, but it is crownward of *Baminornis* that has a pygostyle, demonstrating the complexity of tail evolution. The Early Cretaceous *Zhongornis* was originally described as an avialan

that may have preserved an abbreviated unfused tail (*57*). However, this specimen has been interpreted to have 20 caudal vertebrae and assigned to scansoriopterygids by recent studies (*4*, *9*).

Developmental studies have suggested that pleiotropic effect of relatively few mutations and inflammation can cause tail shortening and fusion of the pygostyle (*9*, *58*), and the coexistence of long- and short-tailed birds shortly after their origins without intermediate forms is not unexpected (*6*, *7*). Therefore, species with transitional morphologies such as an abbreviated and unfused tail have been thought unlikely to have existed (*6*, *7*). However, the discovery of *Zhengheornis* just fills this "hypothetic vacancy" by capturing a previously undocumented intermediate stage with a distally unfused tail consisting of fewer shorter caudal vertebrae (Fig. 4A and figs. S13 and S14), challenging previous hypotheses (*6*).

To trace changes of the tail across non-avialan and avialan theropods transition, we reconstructed the evolution of tail length using phylogentic comparative method. The result shows that *Zhengheornis* has the proportionately shortest tail among non-pygostylian paravians, with its general body plan approaching the derived condition (Fig. 4B and fig. S3). That tail morphology brings aerodynamic benefits: A short tail reduces body weight and results in the anterior shift of the center of mass and lift force (*2*, *59*); fewer caudal vertebrae (fewer number of joints) increase stiffness of the tail that enhances fight control (*60*); and a short tail decreases the lever arm to raise or depress the tail feathers, which contributes stability and maneuverability. Moreover, *Zhengheornis* lacks elongate chevrons, pre- and postzygapophyses of the kind present in other non-avialan theropods and long-tailed avialans such as *Archaeopteryx* and *Anchiornis* (*38*, *60*), making its tail less rigid. Together, *Zhengheornis* demonstrates that the reduction of free caudal counts (from >30 to 15) and the shortening of vertebral bodies occurred prior to the fusion of the pygostyle, disentangling the path of bird tail evolution.

The holotype of *Zhengheornis* is, to our knowledge, the smallest adult individual of non-pygostylian theropods known thus far. Specifically, the femur of IVPP V34168 measures ~63% the length of that of the holotype of *Microraptor zhaoi* (IVPP V12330)—the smallest previously known adult specimen of non-avialan theropods (*61*); the femur is 10% shorter than that of the recently reported Chicago specimen of *Archaeopteryx*, which has been described as the smallest long-tailed avialan (*21*, *26*); and IVPP V34168 is even smaller than the co-occurring short-tailed avialan *Baminornis* (table S3). *Zhengheornis* is smaller than other non-pygostylian theropods, reaching the size class that is accessed by small Early Cretaceous enantiornithines such as *Protopteryx* (Fig. 4C and fig. S4). Miniaturization along the line to avialans contributed to the appearances of some evolutionary novelties including powered flight (*18*, *62*, *63*), and, more importantly, facilitated access to new niches, which have been constrained by threshold of body size (*64*). We investigated changes of body mass across the theropod tree under a phylogenetic comparative framework, focusing on the stage near the origin of avialans. As the smallest known Jurassic paravians, *Zhengheornis* demonstrates that some early-diverging avialans got much smaller earlier in their history than we used to think, which could represent an experimentation with volant behavior. *Zhengheornis*, *Fujianvenator*, and *Baminornis* show disparate bauplans (e.g., long and short tails), body sizes (leg length varies from 107 to 225 mm), and morphologies (e.g., robust and slender ischium, long and short tibia, and non-avialan and ornithothoracine-like pectoral girdle), clearly demonstrating that avialans were already well diversified by the end of Jurassic, supporting the recent macroevolutionary hypothesis that birds were fairly diversified by the end of Jurassic (*11*, *12*, *65*).

MATERIALS AND METHODS

Provenance of IVPP V34168

The holotype specimen of *Zhengheornis buyu* (IVPP V34168) was discovered from the main excavation site of the Zhenghe Fauna [148 to 150 million years ago (Ma)] (*10*), near Yangyuan Village, Zhenghe Country, Nanping City, Fujian Province, in our 2024 fieldwork (from 10 March to 28 April). In addition to IVPP V34168, the Zhenghe Fauna has thus far yielded another three avialans, including *Fujianvenator* (IVPP V31985) (*10*), *Baminornis* (IVPP V33259), and an incomplete specimen represented by only a furcula (IVPP V33260) (*7*). The holotype of *Zhengheornis* and IVPP V33260 were preserved in "layer six," above the horizon ("layer two") that preserves the holotypes of *Fujianvenator* and *Baminornis* [see the composite stratigraphic log in figure 4 in (*10*)]. IVPP V34168 was prepared by a professional technician from the IVPP, under the supervision of the authors. The specimen (IVPP V34168) described in this study is archived and available from the IVPP, Chinese Academy of Sciences, Beijing, China.

Phylogenetic analysis

To investigate the phylogenetic position of IVPP V34168, we performed both maximum parsimony and Bayesian tip-dating analyses using the latest version of Theropod Working Group matrix (TWiG) (*66*) with modifications following recent studies (*7*, *10*, *67*). The revised matrix consists of 169 taxa and 853 morphological characters (data S1 and S2). Maximum parsimony analysis was conducted using the TNT software package (*68*) with the following settings: All characters were equally weighted and analyzed using the New Technology search algorithm with sectorial search, ratchet, tree drift, and tree fusion to find the most parsimonious tree; the minimum-length tree was searched for 20 replicates to find as many tree islands as possible; and the resulting parsimonious trees were fed into a second round of branch swapping using the traditional tree bisection-reconnection method to search treespace more extensively. We calculated the Bremer and the absolute frequency of the bootstrap values as the node-supporting indices. The Bremer support values were calculated using the Bremer script embedded in TNT. The absolute boostrap values were calculated via 1000 replicates using the same setting as the primary search.

The strict consensus was relatively well resolved (length = 3583; consistency index = 0.304; retention index = 0.782). The interrelationships of the major clades are consistent with most recent phylogenetic analyses (fig. S11) (*7*, *10*, *67*). IVPP V34168 was resolved in a stemward position within the Avialae, and it is just crownward of *Archaeopteryx* and the Anchiornithinae. The other two Zhenghe avialans—*Fujianvenator* and *Baminornis*—were recovered in the same phylogenetic position as in previous studies (*7*, *10*), with the former falling within the Anchiornithinae and the latter emerging as the immediate outgroup to the clade uniting *Jeholornis* and more crownward taxa.

Bayesian tip-dating method was performed using the MrBayes (v. 3.2.7b) software (*69*), with same setting as in our previous study (*7*). Mkv model (*70*) with gamma rate variation across characters was used for the morphological characters (*71*). The prior for the

time-calibrated tree was modeled by the fossilized birth-death process (*72*). The root age was assigned an offset-exponential prior with mean age of 180 Ma and minimal age of 170 Ma. The fossil ages were given uniform distributions based on the formations and horizons where the fossils were found. The extant-sampling probability was fixed to 0.0005 based on the number of living birds. The prior for the evolutionary rate was modeled by the uncorrelated lognormal and gamma mixed clock (*73*). The mean evolutionary rate was assigned an exponential prior with mean 0.01 (approximately one change per character per 100 million years), and the variance parameter was given an exponential prior with mean 1.0. Two independent runs and four chains per run (one cold chain and three hot chains with temperature 0.06) were conducted in Markov chain Monte Carlo. Each run was executed 60 million generations and sampled every 2000 generations. The first 25% samples were discarded as burn-in, and the rest from the two runs were combined. Good convergence and mixing were diagnosed by the effective sample size larger than 100 for all parameters and the average standard deviation of split frequencies (*69*) smaller than 0.01. The posterior trees were summarized as a 50% majority-rule consensus tree. IVPP V34168 was resolved within the Avialae and forms the immediate outgroup to the clade encompassing *Baminornis* and more crownward taxa, a result consistent with maximum parsimony analysis (fig. S12).

Laser-stimulated fluorescence photographing

IVPP V34168 was photographed using the laser-stimulated fluorescence method. Photos were taken using a 450-nm, 500-mW blue laser (MDL-III-450-1W, Changchun New Industries Optoelectronics Tech. Co.), with an LP-500-62 light yellow long-pass filter and a Nikon D850.

Phylogenetic comparative analyses

To compare the hindlimb proportion of *Zhengheornis* with that of other Mesozoic theropods (including avialans), we performed phylogeny-based comparative analyses using the lengths of femur, tibia/tibiotarsus, and metatarsal III. Hindlimb proportion is ecological informative and has been widely used to illuminate habitats of extinct vertebrates (*74*–*77*), and thus, our comparative analyses could help understand the ecological adaptation of *Zhengheornis*. A dataset of the length of the hindlimb elements spanning the whole spectrum of Mesozoic theropod phylogeny was compiled based on our direct measurement and the literature (table S8). To circumvent the controversy about the scaling relationships of limb size and ontogenetic impacts, only adult and subadult specimens that preserve the complete length for all three hindlimb elements were included. The length dataset contains 138 species, including all the known Jurassic avialans. An informal supertree that contains all the taxa in the length dataset was constructed in Mesquite (v. 3.61) (*78*), with reference to current and latest phylogenetic analyses (*30*, *41*, *66*, *67*). Branches subtending to taxa with competing phylogenetic positions were collapsed as polytomies. The supertree was time-scaled using tip dates constrained by the first and last appearance datum of the geological formations where the specimens were discovered (*79*). We applied the "minimum branch method" to calibrate the supertree using the timePaleoPhy function in the R package paleotree (*80*). The dated supertree was used as the backbone in downstream analyses.

The length measurements were $\log_{10}$-transformed to normalize the distribution prior to subsequent analyses. To account for the size-dependent limb measurements (*81*), we calculated the residues from a least-squares regression of the $\log_{10}$-transformed length data against body mass using the phyl.resid function of the R package phytools (*82*). Body masses of Mesozoic theropods were estimated using the empirical equation derived from living bipedal tetrapods (*18*). To account for nonindependence in phenotypes (here, body mass and limb measurement) due to shared evolution (*83*), we performed pPCA using the phyl.pca function in the R package phytools (*82*). The size-corrected residuals were fed into pPCA, which reconstructed ancestral states using maximum likelihood under a Brownian model of evolution. The resulting PCs and the phylogeny were used to construct the phylogenetic morphospace, which demonstrated the interrelationships and the direction and magnitude of morphological variations along different branches. PC 1 explains 82.9% of the variance and negatively correlates with all variables, showing that it refers the overall elongation of the leg (body size related) (table S5). As such, Mesozoic avialans are generally separated from the large sized non-avialan therapods along PC 1. *Zhengheornis* plots closer to the morphospace of Cretaceous avialans than other Jurassic avialans along PC 1 (Fig. 3, A to C, and fig. S8A). PC 2 correlates positively with metatarsal III, but negatively with femur and tibia. The high loading of eigenvector coefficients on metatarsal III and femur suggests that PC2 corresponds to the elongation of the metatarsal III relative to the femur. The eigenvector coefficients of PC 3 are negatively related with tibia but positively correlate with the femur and metatarsal III, showing that this axis describes the relative elongation of the tibia. In living birds, terrestrial forms typically have elongate tibiotarsus and tarsometatarsus, because elongate distal elements are functionally beneficial in increasing stride distance, whereas arboreal birds usually have short distal elements, which helps bring their center of body mass close to the substrate (*74*, *77*). In the binary plot of PCs 2 and 3, enantiornithines are generally separated from early ornithuromorphs, with *Zhengheornis* in the intermediate position (fig. S8A). Other Jurassic avialans—*Archaeopteryx*, *Fujianvenator*, and *Anchiornis*—are placed on the more positive end of PC 2 and more negative end of PC 3, respectively (Fig. 3, B and C). *Archaeopteryx*, *Fujianvenator*, and *Anchiornis* are closer to the morphospace of early ornithuromorphs than *Zhengheornis*, suggesting ecological diversification among these taxa. Conventional PCA, which do not account for phylogeny and body size, was also performed for comparison, and comparable results were recovered (fig. S8, C and D, and table S6). pPCA including only avialans produced similar results (fig. S9 and table S7).

To quantify and compare the impact of *Zhengheornis* on the disparity of hindlimb proportion of Jurassic avialans, we calculated three widely used disparity metrics, the sum of ranges and variances, and the median distance from the centroids (*52*, *53*). Ranges describe the overall morphological dispersion and are relatively robust to the bias induced by the splitting of specimens (*53*). Variances capture the average dissimilarity among specimens and are relatively independent from sample size bias (*53*). The median distance from the centroids describes the median Euclidean distance of individual specimens from the centroid of their group (*52*). Disparity metrics were calculated using the PC scores derived from pPCA, which were bootstrapped using 1000 replicates to produce a confidence interval using the R package dispRity (*84*). For intergroup comparison, we divided Mesozoic theropods into four subgroups, Cretaceous avialans ($n = 58$), Jurassic avialans ($n = 6$), non-avialan paravians ($n = 16$), and non-paravian theropods ($n = 58$). We calculated the

disparity metrics with and without *Zhengheornis*, respectively, and then compared the results. The results show that *Zhengheornis* does increase the disparity of Jurassic avialans in terms of sum of ranges but bring little effect in the other two metrics (Fig. 3D). Rarefaction analyses were conducted to estimate how the disparity metrics were affected by the uneven species numbers among these subgroups, using the boot.matrix function in the R package dispRity (*84*).

A ternary diagram of the proportions of the non-ungual phalanges of pedal digit III is a simple and useful method to distinguish tetrapods, particularly birds that are adapted to different habitats, e.g., arboreal and terrestrial (*85*, *86*). We added *Zhengheornis* and other Jurassic avialans ($n = 5$) into the dataset in (*85*), which consists of 183 modern birds that are classified as either arboreal or terrestrial (table S9). The result shows that the five Jurassic avialans plot in the overlap region of arboreal and terrestrial birds, showing that their pedal digits were not specialized to either habitats (fig. S8B). We further conducted discriminant function analysis using the lda function in the R package MASS (*87*). Length measurements of pedal digit III of modern birds were used as the training data, and 81% of modern birds can be accurately assigned to their original ecology using the obtained discriminant function. *Zhengheornis* was assigned to the arboreal group based on the discriminant function.

Body mass estimate and change

Estimation of the body mass of extinct animals is notoriously difficult. Here, we used recently developed methods based on empirical scaling relationships between body mass and limb bone dimensions (*17*, *18*). We first estimated the body mass of IVPP V34168 based on the correlation between body mass and circumference of the femur as in (*18*), which gave a body mass of 73.7 g. Alternatively, we used the equation based on body mass and femur length as in (*17*), which produced a larger value as 162.5 g. Despite the variation of these estimations, the preserved limb elements (e.g., femur, tibia, metatarsus, and ulna) of IVPP V34168 is shorter than that in other non-pygostylian theropods, including the Eichstätt (regarded as a juvenile) and the Chicago specimens of *Archaeopteryx* (table S8). Therefore, we suggest that the holotype of *Zhengheornis* is the smallest individual of long-tailed theropods (juvenile or younger individuals not considered) known thus far. To visualize change of body mass along the line to early avialans, we superimposed the phylogeny and the body mass estimations of Mesozoic theropods using the continuous character mapping method in the R package phytools (*82*). The fancyTree function was applied, which estimated the ancestral states using the maximum likelihood and produced the 95% confidence interval. The result clearly shows that IVPP V34168 expands the known body size diversity of early avialans, and it reaches the size class that was only available to small enantiornithines among the known Mesozoic theropods (Fig. 4C and fig. S14).

Evolution of tail

To investigate change of the tail across the non-avialan and early avialan theropod transition, we compared the number of free caudal vertebrae and tail length using phylogenetic comparative methods. We compiled a dataset that includes, to our knowledge, all the Mesozoic theropods that preserve the complete tail (both the number of caudal vertebrae and entire tail length can be confidently accessed) through exhaustive literature search (table S2). The tail dataset contains 41 species, including 27 Mesozoic avialans and 14 non-avialan theropods (no juvenile or younger individuals considered). The tail length is measured using the freehand method in ImageJ software (v. 1.53g) based on published resources. For specimens that preserve disarticulated caudal vertebrae, the tail length is calculated using the combined length of all caudal vertebrae. For pygostylian birds, the tail length equals the combined length of the free caudals and the pygostyle. A time-scaled informal supertree, which describes the phylogenetic position of the taxa included in the tail dataset, was constructed following the same method outlined above. The length ratio between the tail and femur (the latter as a proxy for body size) was calculated to reflect the relative elongation/abbreviation of the tail. To trace changes of the relative tail length across the phylogeny, the length ratio was mapped on the timed-scaled phylogeny using the fancyTree function in the R package phytools (Fig. 4B and fig. S13) (*82*), which also estimated the ancestral states using the maximum likelihood with 95% confidence interval.

Supplementary Materials

The PDF file includes:

Figs. S1 to S14
Tables S1, S3 to S7
Legends for tables S2, S8 and S9
Data S1 and S2
References

Other Supplementary Material for this manuscript includes the following:

Tables S2, S8 and S9

REFERENCES

1. F. B. Gill, *Ornithology* (W.H. Freeman, ed. 3, 2007).
2. S. M. Gatesy, K. M. Middleton, Bipedalism, flight, and the evolution of theropod locomotor diversity. *J. Vertebr. Paleontol.* **17**, 308–329 (1997).
3. R. N. Felice, P. M. O'Connor, Ecology and caudal skeletal morphology in birds: The convergent evolution of pygostyle shape in underwater foraging taxa. *PLOS ONE* **9**, e89737 (2014).
4. J. K. O'Connor, C. Sullivan, Reinterpretation of the Early Cretaceous maniraptoran (Dinosauria: Theropoda) *Zhongornis haoae* as a scansoriopterygid-like non-avian, and morphological resemblances between scansoriopterygids and basal oviraptorosaurs. *Vertebr. Palasiat.* **52**, 3–30 (2014).
5. S. L. Brusatte, The lost long tail of early bird evolution. *Nature* **638**, 323–324 (2025).
6. D. J. Rashid, S. C. Chapman, The long and the short of tails. *Dev. Dyn.* **250**, 1229–1235 (2021).
7. R. Chen, M. Wang, L. Dong, G. Zhou, X. Xu, K. Deng, L. Xu, C. Zhang, L. Wang, H. Du, G. Lin, M. Lin, Z. Zhou, Earliest short-tailed bird from the Late Jurassic of China. *Nature* **638**, 441–448 (2025).
8. D. Rashid, S. Chapman, H. Larsson, C. Organ, A.-G. Bebin, C. Merzdorf, R. Bradley, J. Horner, From dinosaurs to birds: A tail of evolution. *Evodevo* **5**, 25 (2014).
9. D. J. Rashid, K. Surya, L. M. Chiappe, N. Carroll, K. L. Garrett, B. Varghese, A. Bailleul, J. K. O'Connor, S. C. Chapman, J. R. Horner, Avian tail ontogeny, pygostyle formation, and interpretation of juvenile Mesozoic specimens. *Sci. Rep.* **8**, 9014 (2018).
10. L. Xu, M. Wang, R. Chen, L. Dong, M. Lin, X. Xu, J. Tang, H. You, G. Zhou, L. Wang, W. He, Y. Li, C. Zhang, Z. Zhou, A new avialan theropod from an emerging Jurassic terrestrial fauna. *Nature* **621**, 336–343 (2023).
11. G. T. Lloyd, D. W. Bapst, M. Friedman, K. E. Davis, Probabilistic divergence time estimation without branch lengths: Dating the origins of dinosaurs, avian flight and crown birds. *Biol. Lett.* **12**, 20160609 (2016).
12. X. Xu, Z. Zhou, R. Dudley, S. Mackem, C. M. Chuong, G. M. Erickson, D. J. Varricchio, An integrative approach to understanding bird origins. *Science* **346**, 1253293 (2014).
13. X. Xu, Z. Zhou, C. Sullivan, Y. Wang, D. Ren, An updated review of the middle-late jurassic yanliao biota: Chronology, taphonomy, paleontology and paleoecology. *Acta Geol. Sin.* **90**, 2229–2243 (2016).
14. K. Tamura, N. Nomura, R. Seki, S. Yonei-Tamura, H. Yokoyama, Embryological evidence identifies wing digits in birds as digits 1, 2, and 3. *Science* **331**, 753–757 (2011).
15. H. Hu, J. K. O'Connor, First species of Enantiornithes from Sihedang elucidates skeletal development in Early Cretaceous enantiornithines. *J. Syst. Palaeontol.* **15**, 909–926 (2017).
16. M. Wang, Z. Zhou, A new adult specimen of the basalmost ornithuromorph bird *Archaeorhynchus spathula* (Aves: Ornithuromorpha) and its implications for early avian ontogeny. *J. Syst. Palaeontol.* **15**, 1–18 (2017).

17. D. J. Field, C. Lynner, C. Brown, S. A. F. Darroch, Skeletal correlates for body mass estimation in modern and fossil flying birds. *PLOS ONE* **8**, e82000 (2013).
18. R. B. J. Benson, G. Hunt, M. T. Carrano, N. Campione, Cope's rule and the adaptive landscape of dinosaur body size evolution. *Palaeontology* **61**, 13–48 (2018).
19. O. W. Rauhut, C. Foth, H. Tischlinger, The oldest *Archaeopteryx* (Theropoda: Avialiae): A new specimen from the Kimmeridgian/Tithonian boundary of Schamhaupten, Bavaria. *PeerJ* **6**, e4191 (2018).
20. D. Hu, J. A. Clarke, C. M. Eliason, R. Qiu, Q. Li, M. D. Shawkey, C. Zhao, L. D'Alba, J. Jiang, X. Xu, A bony-crested Jurassic dinosaur with evidence of iridescent plumage highlights complexity in early paravian evolution. *Nat. Commun.* **9**, 217 (2018).
21. G. Mayr, B. Pohl, S. Hartman, D. S. Peters, The tenth skeletal specimen of *Archaeopteryx*. *Zool. J. Linn. Soc.* **149**, 97–116 (2007).
22. R. Pei, Q. Li, Q. Meng, M. A. Norell, K.-Q. Gao, New specimens of *Anchiornis huxleyi* (Theropoda: Paraves) from the Late Jurassic of northeastern China. *Bull. Am. Mus. Nat. Hist.* **411**, 1–67 (2017).
23. P. Godefroit, A. Cau, H. Dong-Yu, F. Escuillie, W. Wenhao, G. Dyke, A Jurassic avialan dinosaur from China resolves the early phylogenetic history of birds. *Nature* **498**, 359–362 (2013).
24. Z. Zhou, F. Zhang, *Jeholornis* compared to *Archaeopteryx*, with a new understanding of the earliest avian evolution. *Naturwissenschaften* **90**, 220–225 (2003).
25. P. Wellnhofer, A short history of research on *Archaeopteryx* and its relationship with dinosaurs. *Geol. Soc. Lond. Spec. Publ.* **343**, 237–250 (2010).
26. J. K. O'Connor, A. Clark, P. C. Kuo, Y. Kiat, M. Fabbri, A. Shinya, C. Van Beek, J. Lu, M. Wang, H. Hu, Chicago *Archaeopteryx* informs on the early evolution of the avian bauplan. *Nature* **641**, 1201–1207 (2025).
27. U. Lefèvre, A. Cau, A. Cincotta, D. Hu, A. Chinsamy, F. Escuillié, P. Godefroit, A new Jurassic theropod from China documents a transitional step in the macrostructure of feathers. *Naturwissenschaften* **104**, 74 (2017).
28. X. Xu, P. Currie, M. Pittman, L. Xing, Q. Meng, J. Lü, D. Hu, C. Yu, Mosaic evolution in an asymmetrically feathered troodontid dinosaur with transitional features. *Nat. Commun.* **8**, 14972 (2017).
29. D. W. E. Hone, Variation in the tail length of non-avian dinosaurs. *J. Vertebr. Paleontol.* **32**, 1082–1089 (2012).
30. A. H. Turner, P. J. Makovicky, M. A. Norell, A review of dromaeosaurid systematics and paravian phylogeny. *Bull. Am. Mus. Nat. Hist.* **371**, 1–206 (2012).
31. X. Xu, H. You, K. Du, F. Han, An *Archaeopteryx*-like theropod from China and the origin of Avialae. *Nature* **475**, 465–470 (2011).
32. P. J. Makovicky, M. A. Norell, "Troodontidae," in *The Dinosauria*, B. W. David, D. Peter, O. Halszka, Eds. (University of California Press, 2004), pp. 184–195.
33. M. A. Norell, P. J. Makovicky, "Dromaosauridae," in *The Dinosauria*, B. W. David, D. Peter, O. Halszka, Eds. (University of California Press, 2004), pp. 196–209.
34. M. Wang, J. K. O'Connor, X. Xu, Z. Zhou, A new Jurassic scansoriopterygid and the loss of membranous wings in theropod dinosaurs. *Nature* **569**, 256–259 (2019).
35. D. Hu, L. Hou, L. Zhang, X. Xu, A pre-*Archaeopteryx* troodontid theropod from China with long feathers on the metatarsus. *Nature* **461**, 640–643 (2009).
36. C. Foth, H. Tischlinger, O. W. M. Rauhut, New specimen of *Archaeopteryx* provides insights into the evolution of pennaceous feathers. *Nature* **511**, 79–82 (2014).
37. F. Zhang, Z. Zhou, X. Xu, X. Wang, C. Sullivan, A bizarre Jurassic maniraptoran from China with elongate ribbon-like feathers. *Nature* **455**, 1105–1108 (2008).
38. W. S. Persons, P. J. Currie, Dragon tails: Convergent caudal morphology in winged archosaurs. *Acta Geol. Sin.* **86**, 1402–1412 (2012).
39. L. M. Chiappe, S. A. Ji, Q. Ji, M. A. Norell, Anatomy and systematics of the Confuciusornithidae (Theropoda: Aves) from the Late Mesozoic of northeastern China. *Bull. Am. Mus. Nat. Hist.* **242**, 1–89 (1999).
40. M. Wang, Z. Zhou, J. K. O'Connor, N. V. Zelenkov, A new diverse enantiornithine family (Bohaiornithidae fam. nov.) from the Lower Cretaceous of China with information from two new species. *Vertebr. Palasiat.* **52**, 31–76 (2014).
41. Z. Li, M. Wang, T. A. Stidham, Z. Zhou, Decoupling the skull and skeleton in a Cretaceous bird with unique appendicular morphologies. *Nat. Ecol. Evol.* **7**, 20–31 (2023).
42. M. M. Rhodes, D. M. Henderson, P. J. Currie, Maniraptoran pelvic musculature highlights evolutionary patterns in theropod locomotion on the line to birds. *PeerJ* **9**, e10855 (2021).
43. Z. Zhou, F. Zhang, A long-tailed, seed-eating bird from the Early Cretaceous of China. *Nature* **418**, 405–409 (2002).
44. M. Wang, Z. Zhou, C. Sullivan, A fish-eating enantiornithine bird from the Early Cretaceous of China provides evidence of modern avian digestive features. *Curr. Biol.* **26**, 1170–1176 (2016).
45. J. F. Botelho, D. Smith-Paredes, S. Soto-Acuña, J. K. O'Connor, V. Palma, A. O. Vargas, Molecular development of fibular reduction in birds and its evolution from dinosaurs. *Evolution* **70**, 543–554 (2016).
46. P. Vickers-Rich, L. M. Chiappe, S. Kurzanov, "The enigmatic birdlike dinosaur *Avimimus portentosus*: Comments and a pictorial atlas," in *Mesozoic Birds: Above the Heads of Dinosaurs*, L. M. Chiappe, L. M. Witmer, Eds. (University of California Press, 2002), pp. 65–86.
47. J. F. Botelho, D. Smith-Paredes, S. Soto-AcuñA, D. NúñEz-LeoN, V. Palma, A. O. Vargas, Greater growth of proximal metatarsals in bird embryos and the evolution of hallux position in the grasping foot. *J. Exp. Zool.* **328**, 106–118 (2016).
48. L. Ossa-Fuentes, S. Soto-Acuña, P. Bona, M. Sallaberry, A. O. Vargas, Developmental evolution of the distal ankle in the dinosaur–bird transition. *J. Exp. Zool.* **338**, 119–128 (2020).
49. S. Hattori, Evolution of the hallux in non-avian theropod dinosaurs. *J. Vertebr. Paleontol.* **36**, e1116995 (2016).
50. X. Xu, X. L. Wang, Troodontid-like pes in the dromaeosaurid *Sinornithosaurus*. *Paleont. Soc. Korea Spec. Publ.* **2000**, 179–188 (2000).
51. L. M. Chiappe, Q. Meng, *Birds of Stone: Chinese Avian Fossils from the Age of Dinosaurs* (Johns Hopkins Univ. Press, 2016).
52. M. A. Wills, E. G. B. Derek, R. A. Fortey, Disparity as an evolutionary index: A comparison of cambrian and recent arthropods. *Paleobiology* **20**, 93–130 (1994).
53. M. Foote, Morphological and taxonomic diversity in a clade's history: The blastoid record and stochastic simulations. *Paleontol. Univ. Mich.* **28**, 101–140 (1991).
54. S. L. Brusatte, J. K. O'Connor, E. D. Jarvis, The origin and diversification of birds. *Curr. Biol.* **25**, R888–R898 (2015).
55. A. L. R. Thomas, On the aerodynamics of birds' tails. *Philos Trans. R. Soc. Lond. B Biol. Sci.* **340**, 361–380 (1993).
56. J. K. O'Connor, L. M. Chiappe, A. Bell, "Pre-modern birds: Avian divergences in the Mesozoic," in *Living Dinosaurs: The Evolutionary History of Birds*, J. D. Gareth, K. Gary, Eds. (Wiley, 2011), pp. 39–114.
57. C. Gao, L. M. Chiappe, Q. Meng, J. K. O'Connor, X. Wang, X. Cheng, J. Liu, A new basal lineage of Early Cretaceous birds from China and its implications on the evolution of the avian tail. *Palaeontology* **51**, 775–791 (2008).
58. D. J. Rashid, J. R. Sheheen, T. Huey, K. Surya, J. B. Sanders, J. R. Horner, J. Voyich, S. C. Chapman, Nonpathological inflammation drives the development of an avian flight adaptation. *Proc. Natl. Acad. Sci. U.S.A.* **120**, e2219757120 (2023).
59. A. M. Heers, K. P. Dial, From extant to extinct: Locomotor ontogeny and the evolution of avian flight. *Trends Ecol. Evol.* **27**, 296–305 (2012).
60. D. W. E. Hone, W. S. Persons, S. C. Le Comber, New data on tail lengths and variation along the caudal series in the non-avialan dinosaurs. *PeerJ* **9**, e10721 (2021).
61. X. Xu, Z. Zhou, X. Wang, The smallest known non-avian theropod dinosaur. *Nature* **408**, 705–708 (2000).
62. M. S. Y. Lee, A. Cau, D. Naish, G. J. Dyke, Sustained miniaturization and anatomical innovation in the dinosaurian ancestors of birds. *Science* **345**, 562–566 (2014).
63. F. E. Novas, M. D. Ezcurra, F. L. Agnolin, D. Pol, R. Ortiz, New Patagonian Cretaceous theropod sheds light about the early radiation of Coelurosauria. *Rev. Mus. Argent. Cienc. Nat.* **14**, 57–81 (2012).
64. J. H. Brown, *Macroecology* (University of Chicago Press, Chicago, 1995).
65. O. W. M. Rauhut, C. Foth, "The origin of birds: Current consensus, controversy, and the occurrence of feathers," in *The Evolution of Feathers: From their Origin to the Present*, C. Foth, O. W. M. Rauhut, Eds. (Springer International Publishing, 2020), pp. 27–45.
66. S. L. Brusatte, G. T. Lloyd, S. C. Wang, M. A. Norell, Gradual assembly of avian body plan culminated in rapid rates of evolution across the dinosaur-bird transition. *Curr. Biol.* **24**, 2386–2392 (2014).
67. A. H. Turner, S. Montanari, M. A. Norell, A new dromaeosaurid from the Late Cretaceous Khulsan locality of Mongolia. *Am. Mus. Novit.* **2020**, 1–48 (2021).
68. P. A. Goloboff, S. A. Catalano, TNT version 1.5, including a full implementation of phylogenetic morphometrics. *Cladistics* **32**, 221–238 (2016).
69. F. Ronquist, M. Teslenko, P. Van Der Mark, D. L. Ayres, A. Darling, S. Höhna, B. Larget, L. Liu, M. A. Suchard, J. P. Huelsenbeck, MrBayes 3.2: Efficient Bayesian phylogenetic inference and model choice across a large model space. *Syst. Biol.* **61**, 539–542 (2012).
70. P. O. Lewis, A likelihood approach to estimating phylogeny from discrete morphological character data. *Syst. Biol.* **50**, 913–925 (2001).
71. Z. Yang, Maximum likelihood phylogenetic estimation from DNA sequences with variable rates over sites: Approximate methods. *J. Mol. Evol.* **39**, 306–314 (1994).
72. C. Zhang, T. Stadler, S. Klopfstein, T. A. Heath, F. Ronquist, Total-evidence dating under the fossilized birth–death process. *Syst. Biol.* **65**, 228–249 (2015).
73. C. Zhang, Selecting and averaging relaxed clock models in Bayesian tip dating of Mesozoic birds. *Paleobiology* **48**, 340–352 (2022).
74. S. M. Gatesy, Hind limb scaling in birds and other theropods: Implications for terrestrial locomotion. *J. Morphol.* **209**, 83–96 (1991).
75. T. A. Dececchi, H. C. E. Larsson, Assessing arboreal adaptations of bird antecedents: Testing the ecological setting of the origin of the avian flight stroke. *PLOS ONE* **6**, e22292 (2011).
76. A. Stoessel, B. M. Kilbourne, M. S. Fischer, Morphological integration versus ecological plasticity in the avian pelvic limb skeleton. *J. Morphol.* **274**, 483–495 (2013).
77. A. Zeffer, L. C. Johansson, Å. Marmebro, Functional correlation between habitat use and leg morphology in birds (*Aves*). *Biol. J. Linn. Soc. Lond.* **79**, 461–484 (2003).

78. W. Maddison, D. Maddison, Mesquite: A modular system for evolutionary analysis, version 3.61 (2019); www.mesquiteproject.org.
79. S. L. Brusatte, "Calculating the tempo of morphological evolution: Rates of discrete character change in a phylogenetic context," in *Computational Paleontology*, A. M. T. Elewa, Ed. (Springer-Verlag, 2011), pp. 53–74.
80. D. W. Bapst, paleotree: An R package for paleontological and phylogenetic analyses of evolution. *Methods Ecol. Evol.* **3**, 803–807 (2012).
81. L. J. Revell, Size-correction and principal components for interspecific comparative studies. *Evolution* **63**, 3258–3268 (2009).
82. L. J. Revell, phytools 2.0: An updated R ecosystem for phylogenetic comparative methods (and other things). *PeerJ* **12**, e16505 (2024).
83. J. Felsenstein, Phylogenies and the comparative method. *Am. Nat.* **125**, 1–15 (1985).
84. T. Guillerme, dispRity: A modular R package for measuring disparity. *Methods Ecol. Evol.* **9**, 1755–1763 (2018).
85. J. A. Hopson, "Ecomorphology of avian and nonavian theropod phalangeal proportions: Implications for the arboreal versus terrestrial origin of bird flight" in *New Perspectives on the Origin and Early Evolution of Birds*, J. Gauthier, L. F. Gall, Eds. (Yale Univ. Press, 2001), pp. 221–235.
86. Z. Zhou, J. O. Farlow, "Flight capability and habits of *Confuciusornis*," in *New Perspectives on the Origin and Early Evolution of Birds*, J. Gauthier, L. F. Gall, Eds. (Yale Univ. Press, 2001), pp. 237–254.
87. W. N. Venables, B. D. Ripley, *Modern Applied Statistics with S* (Springer, 2002).
88. M. J. Motta, F. Brissón Egli, F. E. Novas, Tail anatomy of *Buitreraptor gonzalezorum* (Theropoda, Unenlagiidae) and comparisons with other basal paravians. *Cretac. Res.* **83**, 168–181 (2018).
89. M. Wang, J. K. O'Connor, Y. Pan, Z. Zhou, A bizarre Early Cretaceous enantiornithine bird with unique crural feathers and an ornithuromorph plough-shaped pygostyle. *Nat. Commun.* **8**, 14141 (2017).

Acknowledgments: We thank W.-Q. Feng, Y. Li, S. Miao, J.-T. Feng, X. Lin, J.-L. Zhang, and L.-C Wang for helping in fieldwork, Y. Li for specimen preparation, W. Gao for photograph preparation, and S. Miao and J.-T. Feng for laser-stimulated fluorescence photograph preparation. **Funding:** This work was supported by the National Natural Science Foundation of China (42225201 to M.W., 42288201 to Z.Z and M.W.); the Key Research Program of Frontier Sciences, CAS (ZDBS-LY-DQC002 to M.W.); the Tencent Foundation (through the XPLORER PRIZE to M.W.); the investigation of the geological relics and fossil resources of the Late Mesozoic basins in western Fujian (Fujian Provincial Department of Natural Resources, GY20220108 to J.T., L.X., K.D., M.L., H.D., G.L., and R.C.); the survey, excavation, and research of paleontological resources in Daxi Village, Zhenghe County; scientific research project of Fujian Provincial Geological Bureau; and the investigation of protection status and evaluation of key paleontological fossil producing areas in Fujian (Fujian Provincial Department of Natural Resources, [350001]FJGC[GK]2023036 to J.T., L.X., K.D., M.L., H.D., G.L., and R.C.). **Author contributions:** Conceptualization: M.W., Z.Z., and J.T. Project administration: M.W. and Z.Z. Writing—original draft: M.W. and J.T. Writing—review and editing: M.W., Z.Z., X.X., J.T., and K.D. Funding acquisition: M.W. and Z.Z. Methodology: M.W. and C.Z. Investigation: M.W., K.D., L.D., G.L., L.X., M.L., Z.Z., J.T., H.D., and R.C. Supervision: M.W. and Z.Z. Resource: M.W., L.D., and J.T. Software: M.W. and C.Z. Validation: M.W., J.T., and X.X. Data curation: M.W. and J.T. Formal analysis: M.W. and J.T. Visualization: M.W. and J.T. **Competing interests:** All authors declare they have no competing interests. **Data, code, and materials availability:** The specimen (IVPP V34168) described in this study is archived and available from the IVPP, Chinese Academy of Sciences, Beijing, China. All data and code needed to evaluate and reproduce the results of this study, including the measurements and phylogenetic matrix that support the findings of this research, are included in the paper, the Supplementary Materials, or the Dryad repository. The MrBayes commands, R code, and raw data used in phylogenetic and morphometric analyses are available at Dryad (http://datadryad.org/share/OGFAiagcdHMLaBDjlPzzxLUEqEb7_H13O9d6Qh9K_G8).

Submitted 15 August 2025
Accepted 22 May 2026
Published 1 July 2026
10.1126/sciadv.aeb5202

Jurassic avialan reveals stepwise evolution of bony tail in birds

Min Wang, Jianrong Tang, Ke Deng, Liping Dong, Liming Xu, Xing Xu, Min Lin, Honggang Du, Ganmin Lin, Runsheng Chen, Chi Zhang, and Zhonghe Zhou

Sci. Adv. **12** (27), eaeb5202. DOI: 10.1126/sciadv.aeb5202